Materials Today Bio 21 (2023) 100732

Contents lists available at ScienceDirect

Materials Today Bio

journal homepage: www.journals.elsevier.com/materials-today-bio

Mechano-biomimetic hydrogel 3D cell cultivation as a strategy to improve mammalian cell protein expression

Yi Zhang [a,1], Si-yang Li [b,c,1], Hang-ju Zhu [d,1], Jun-Wei Lai [b,c], Shuo-shuo Sun [e], Yue Lin [e], Xing-ling Li [b,c], Zhao-bin Guo [f], Ziheng Lv [e], Hongxu Meng [g], Ke Hu [e,*], Ming Xu [h,i,j,k,l,**], Ting-ting Yu [b,c,j,k,***]

[a] Department of Colorectal Surgery, The First Affiliated Hospital of Nanjing Medical University, Nanjing, 210029, Jiangsu, China
[b] Department of Medical Genetics, School of Basic Medical Science, Nanjing Medical University, Nanjing, 211166, Jiangsu, China
[c] Jiangsu Key Laboratory of Xenotransplantation, Nanjing Medical University, Nanjing, 211166, Jiangsu, China
[d] Jiangsu Cancer Hospital, The Affiliated Cancer Hospital of Nanjing Medical University, Nanjing, 210009, Jiangsu, China
[e] Department of Biomedical Engineering, School of Biomedical Engineering and Informatics, Nanjing Medical University, Nanjing, 210009, Jiangsu, China
[f] Institute of Interdisciplinary Integrative Medicine Research, Shanghai University of Traditional Chinese Medicine, Shanghai, 201203, China
[g] Zhejiang University-University of Edinburgh Institute, Zhejiang University School of Medicine, Zhejiang University, Hangzhou, 314400, China
[h] Engineering Research Center of Health Emergency, Jiangsu Provincial Center for Disease Control and Prevention, Nanjing, 210009, China
[i] Jiangsu Province Engineering Research Center of Health Emergency, Nanjing, 210009, China
[j] Jiangsu Preventive Medicine Association, Nanjing, 210009, China
[k] School of Public Health, Nanjing Medical University, Nanjing, 211166, China
[l] Department of Pharmaceutics, School of Pharmacy, Nanjing Medical University, Nanjing, 211166, Jiangsu, China

ARTICLE INFO

Keywords:
Eukaryotic protein expression
3D cell culture
Cellular physical microenvironment
Hydrogel

ABSTRACT

Eukaryotic expression systems are frequently employed for the production of recombinant proteins as therapeutics as well as research tools. Among which mammalian cell protein expression approach is the most powerful one, which can express complex proteins or genetic engineered biological drugs, such as PD-1. However, the high expense, which partially derives from its low protein yielding efficiency, limited the further application of such approach in large scale production of target proteins. To address this issue, we proposed a novel technique to promote the protein production efficiency of mammal cells without using conventional genetic engineered approaches. By placing 293T cells in a hydrogel 3D cell culture platform and adjusting the stress relaxation of the matrix hydrogel, cells formed multicellular spheroids by self-organization. In particular, the multicellular spheroids have a significantly enhanced ability to transiently express multiple proteins (SHH–N, PD-1 and PDL-1). We also examined in detail the mechanism underlying this phenomenon, and found that the reorganization of cytoskeleton during spheroids formation enhances the translation process of protein by recruiting ribosomes. Overall, this finding provides a novel approach for subsequent improvement of large-scale mammalian protein expression cell systems.

1. Introductions

Eukaryotic expression technology is a commonly used approach for expressing recombinant proteins in recent years [1]. It complements the features lacking in the classical prokaryotic protein expression system, such as the ability to form stable disulfide bonds when the protein is expressed, and the ability to modify the protein properly after translation so that the expressed protein is more naturally active rather than being degraded or forming inclusion bodies [2] Eukaryotic protein expression systems include mammalian cell protein expression systems, yeast protein expression systems, and insect protein expression systems [3]. Among them, the mammalian cell protein system is a platform for

* Corresponding author.
** Corresponding author.Engineering Research Center of Health Emergency, Jiangsu Provincial Center for Disease Control and Prevention, Nanjing, 210009, China.
*** Corresponding author.Department of Medical Genetics, School of Basic Medical Science, Nanjing Medical University, Nanjing, 211166, Jiangsu, China.
E-mail addresses: kehu@njmu.edu.cn (K. Hu), sosolou@jscdc.cn (M. Xu), tingting@njmu.edu.cn (T.-t. Yu).
[1] These authors contributed equally to this paper.

https://doi.org/10.1016/j.mtbio.2023.100732
Received 31 March 2023; Received in revised form 23 June 2023; Accepted 12 July 2023
Available online 14 July 2023
2590-0064/© 2023 Published by Elsevier Ltd. This is an open access article under the CC BY-NC-ND license (http://creativecommons.org/licenses/by-nc-nd/4.0/).

the production of genetically engineered drugs and is suitable for the discovery of new genes and the study of protein structure and function [4]. It is the most expensive eukaryotic expression system but the only one that can express complex protein genes, suitable for proteins such as sonic hedgehog (Shh), programmed cell death protein 1 (PD-1), etc. that need to be modified by glycosylation to exert biological effects [5]. If the current commonly used protein expression system can be improved, it can not only create a huge economic effect but also solve the problem of insufficient supply of some proteins in clinical and research, by increasing the protein expression and improving the quality of the expressed proteins.

The existing mammalian cell expression systems are mainly based on adherent cells or suspension cells [6]. Small-scale culture of walled cells can be done in cell dishes or cell bottles, while large-scale culture requires cells to be resuspended in medium and transferred to bioreactors lined with sufficient number of microcarriers. However, the yield of the mammalian cell expression system (0.2–200 mg/L) [7] is still much lower than that of the prokaryotic cell protein expression system (10–30% of total cellular protein) [8], and also lower than that of the comparable yeast cell protein expression system (1–30% of total cellular protein) [9] and insect cell protein expression system (1–500 mg/L) [10].

Currently, strategies to improve mammalian cell expression systems to enhance protein synthesis are mainly focused on (i) host cell engineering. For example, anti-cell death engineering of CHO cells or genetic glycoengineering in mammalian cells to increase the integrated viable cell density (IVCD) and cell-specific productivity; (ii) construction of efficient expression vectors. Such as introducing co-amplified genes, constructing expression vectors with different combinations of regulatory elements, weakening screening tags, etc. to improve the level of recombinant protein expression; (iii) high-throughput cloning workflow to obtain high-yielded clones; (iv) optimize the culture process and cell culture media, for example, by starting with media of chemically-defined composition and incorporating cell type-specific growth factors. To meet the increasing demand for scientific research, drug development, and therapeutic applications of protein drugs, it is necessary that innovating the production process with a higher production capacity, high quality product, and reducing production costs.

The physical microenvironment in which cells are grown has a significant impact on affecting cell phenotype and function, and many biomaterials have been developed to modulate cell function through their biomechanical properties [11]. In our previous study, we developed a series of 3D cell culture platforms based on composite hydrogels with tunable mechanical properties and cell adhesion capacity and found that the ability of beta islet cells to synthesize and secrete insulin was significantly enhanced by modulating the physical microenvironment of the cells [12], based on which we hypothesized that altering the characteristic biomechanical properties of the hydrogels might change the metabolism of the cells as well as the form of self-organization performance of mammalian cells as protein expression vectors. In this study, we propose a mammalian protein expression technique based on a hydrogel 3D cell culture platform to promote 293T cells, which has been extensively used as an expression tool for recombinant proteins since it was generated over 35 years ago, to form multicellular spheroids through self-organization by altering the stress relaxation of the hydrogel. To evaluate the protein expression ability of 293T multicellular spheroids, transient expression of Shh-N (N-terminal fragment of Shh), PD-1 and programmed cell death 1 ligand 1 (PDL-1) were tested, since the efficient expression of these proteins is of great importance for the development of SHH signaling pathway inhibitors and monoclonal antibodies that target either PD-1 or PD-L1, which are currently hot issues in field of tumor-targeted therapy. The 293T multicellular spheroids cultured using this technique have a significantly enhanced ability to transiently express multiple proteins [(SHH–N, PD-1 and PDL-1] with universal application, providing a new idea for subsequent improvement of large-scale mammalian protein expression cell systems.

2. Materials and methods

2.1. Preparation of the GelMA/PEGDA composite hydrogel

Polyethylene glycol diacrylate (Shanghai Aladdin Bio-Chem Technology Co., LTD, 2000 Mw, PEGDA, 1% w/w), Methacrylated Gelatin (Jiangyin StemEasy Biotechnology Company, 20% substitution, GelMA, 10% w/w), and N,N dimethyl bisacrylamide (Shanghai Aladdin Bio-Chem Technology Co., LTD, MBAA, 0.25% w/w) were dispersed in deionized water. For composite hydrogel with as control group, PEGDA (2000 Mw, 0.5%w/w), GelMA (20% substitution, 10% w/w), MBAA (1.25% w/w) were dispersed in deionized water. The mixture was stirred at 60 °C for 2 h until all components were completely dissolved and residual impurities was removed. Lithium phenyl-2,4,6-trimethylbenzoylphosphonate (Jiangyin StemEasy Biotechnology Company, LAP1% w/w) was added to the solution and sonicated until completely dissolved, and impurities were removed by rapid filtration. Then light polymerization (wavelength 405 nm, light intensity 500 mW/cm^2, 5 min) was carried out after pre-polymerization solution was injected into a mold. All the chemicals were purchased from Sigma-Aldrich unless otherwise stated.

2.2. Mechanical properties characterization of hydrogel

Young's modulus and stress relaxation of hydrogels were characterized by a nanoindenter (Piuma, Optics11, The Netherlands). The spherical optical probe of the nanoindenter has a tip radius of 10 μm and a stiffness of 0.43 N m^{-1}. When measuring Young's modulus, the probe was set to press in 10 μm within 2 s and to unload after holding for 1 s, (25-point plotting). The probe was set to press in 15 μm in 5 s when measuring stress relaxation and unload after holding for 200 s.

2.3. Cell lines and antibodies

HEK-293T cells (293T) were purchased from ATCC. Mouse embryo fibroblasts (MEFs) were a gifts from Jin-ke Cheng at the Department of Biochemistry and Molecular Cell Biology (Shanghai Jiao Tong University School of Medicine, Shanghai, China). 293T and MEFs were cultured in Dulbecco's Modified Eagle Medium (Thermo Fisher Scientific, Waltham, MA, 12800017) containing 10% fetal bovine serum (Thermo Fisher Scientific, Waltham, MA, 10270-106), 2 mM L-glutamine (Thermo Fisher Scientific, Waltham, MA, 35050061), 1 mM Sodium Pyruvate (Thermo Fisher Scientific, Waltham, MA, 35050061) and 1 × Penicillin, Streptomycin and Neomycin Antibiotic Mixture (Thermo Fisher Scientific, Waltham, MA, 15640055). Antibodies used in this study are listed in Supplemental Table S1. The secondary antibodies were horse radish peroxidase-conjugated antibodies from Santa Cruz Biotechnology (1:5000 for Western analysis) and Alexa Fluor-conjugated antibodies from Thermo Fisher Scientific (1:200 for IF, A-21206, A-21207, A-21203).

2.4. Preparation of SHH-N enriched medium

ShhN conditioned medium was prepared from 293T cells transfected with a plasmid expressing the amino signaling domain of Shh (RK5-Shh-N plasmid). In brief, 2D cultured 293T cells were transfected with RK5-Shh-N plasmid (only express the N-terminus of SHH protein with signal pathway activation activity) or an empty plasmid as control in strict accordance with the manufacturer's instructions (Genebank Biosciences Inc., GB1001). 24 h after transfection, the cells were reseeded in 2D plate or on hydrogel to form multicellular spheroids (MCSs). Cell culture medium was replaced with 2% FBS low-serum medium. The supernatants containing secreted Shh-N of 2D or 3D cultured 293T cells were collected 72 h after reseeding by centrifugation (800 rpm, 4min) and then filtered through a 0.22 μm filter membrane (Merck Millipore Ltd., SLGPR33RB) immediately. The supernatant was aliquoted and stored at

−80 °C until further use.

2.5. Quantification of Shh-N

SHH-N in the supernatants were analyzed by an enzyme-linked immunosorbent assay (ELISA) using mouse Sonic Hedgehog/SHH N-Terminus Quantikine ELISA Kit (R&D systems, MSHH00), according to the manufacturer's protocol.

The cells cultured under different conditions were collected and lysed for protein quantification using a bicinchoninic acid (BCA) assay. The results of SHH-N ELISA were normalized to the amount of protein from the corresponding cells. The BCA assay was performed on the cell spheroid post-lysis, according to the manufacturer's instructions (Thermo Fisher Scientific, Waltham, MA, 23225).

2.6. Immunofluorescence

For MEFs, cells were seeded on glass coverslips (NEST, 801007) in 12-well plates and starved in DMEM (Dulbecco's modified Eagle's medium) containing 0.5% fetal bovine serum for 24 h before treatment with SHH-N conditional medium (SHH–N-CM) diluted 10 times with serum-free DMEM. The cells were washed three times with phosphate buffered saline (PBS, Solarbio, Beijing, P1000), then fixed with 4% paraformaldehyde (PFA, Solarbio, Beijing, P1110) at room temperature for 30 min. All samples were permeabilized and blocked for 30 min at 4 °C with 3% bovine serum albumin (BSA, BioFroxx, 4240GR100) in 0.3% Triton X-100 (Biosharp, BS084)/PBS. Blocking and subsequent steps were performed in a moist chamber to avoid sample drying. Cells were incubate with primary antibodies (diluted in 3%BSA/0.3%Trition X-100/PBS) for 12 h at 4 °C. After 3 × 10 min washed with 1% Tween (Sigma, V900548) in tris buffered saline (TBS), cells grown on glass coverslips were incubated in dark for 1 h at room temperature with secondary antibodies conjugated to fluorescent dyes (diluted in 3%BSA/0.3%Trition X-100/PBS) and wash the secondary antibodies just like the primary antibodies. For DNA staining, all samples were mounted with DAPI (4′,6-Diamidino-2-phenylindole, Sigma, F6057) for 2 h at room temperature. For 293T, cells were seeded on glass coverslips prepossessed by poly-D-lysine (Sigma-Aldrich, P0899) over 30 min for regularly cultivated overnight, then fixed with 4% PFA. The lipid molecules of cell membrane structure were labeled with lipophilic dye CM-DiI (Yeasen, 40718ES50). For F-ACTIN staining, all samples were mounted with phalloidin (YEASEN, 40734ES75) and standard procedures for immunostaining were followed. Confocal images of the primary cilium were acquired. The percentage of cells with cilia was calculated by randomly counting over 50 cells in each of the three triplicated glass coverslips. Quantification of the fluorescence intensity of *Smo* and *Gli2* in primary cilia was carried out using Image-Pro as described previously [13].

2.7. 293T MCSs freezing slices

293T cells were spheroid cultured in the Ultra-low attachment surface polystyrene (Corning, 3471) for 3 days, the 293T cells were assembled and forming spheroids. Rinsed by PBS, the collected spheroids were fixed in 4% PFA for 24 h at 4 °C, and then embedded in optimum cutting temperature (OCT) compound (Tissue-Tek, Sakura Finetek, Japan, 4583). Attention should be paid to gentle operation for incompact spheroids. Frozen in Cryostat at −20 °C until crystal substantial, the sections were sliced with a thickness of 9 μm, and then collected on adhesive microscope slides (CITOTEST, 188105), and standard procedures for immunostaining were followed.

2.8. Reverse transcription (RT) and real-time PCR

Total RNAs were isolated from cultured cells with RNAiso Plus reagent (TaKaRa, 9109) and reverse transcribed using HiScript II Q RT SuperMix (Vazyme, Q233-01). Quantitative real-time PCR (qPCR) was carried out using AceQ qPCR SYBR Green Master Mix (Vazyme, Q111-02). For each data point, triplicate reactions were carried out and the experiment was repeated three times to assess the statistical significance. RT-qPCR primer sequences can be followed in Supplemental Table S2.

2.9. SHH-N ligand activity assay

MEF cells were seeded on the plate and cultured in cell cultured incubator for 24 h. After that, the cells were transfected with 8 × GLI-luciferase reporter plasmid (was a gift from Dr. Chichung Hui from the University of Toronto) and control reporter plasmid (pRL-TK, Promega) at a ratio of 9:1 in strict accordance with the requirements of the transfection instructions (Polyplus, CPT_114), incubate in cell incubator for 24 h. Treating MEFs with SHH-N, SHH-N-CM, SHH produced by the CHO eukaryotic system (genscript, Z02990), and produced by the E.coil. prokaryotic system (genscript, Z03008), the cells were cultured with successively diluted with serum-free DMEM for 24 h. The dual luciferase reporter assay follows the manufacturer's protocol (Vazyme, DL101-01). The final reading of dual luciferase detected by 96 microplate luminometer (Promega, GloMax).

2.10. Polysome profiling

This procedure was performed according to previous reports [14]. Briefly, SHH-N overexpression 293T cells were cultured in 2D plate adherent cultured and 3D cultured to form MCSs for 1 day respectively. Cells were treated with 100 μg/ml cycloheximide (EMD Millipore Corp., 239763) in serum-containing culture medium for 30 min. After incubate in cell incubator cells were washed with ice-cold PBS containing 100 μg/ml cycloheximide. The harvested cells were centrifuged at 800 × rpm for 4 min and collect into cell cryopreservation. The cells were quickly frozen by liquid nitrogen and stored at −80 °C if necessary. The cell pellets were suspended with 200 μl of ice-cold lysis buffer containing 40 unit/ml DNase inhibitor and PMSF. After 30 min incubation on ice lysates were centrifuged at 13000×*g* at 4 °C for 10 min to separate the cell debris. The cytoplasmic lysate was layered onto a linear gradient of 10%–45% sucrose and centrifuged in an SW40 rotor at 36000 × rpm at 4 °C for 3 h. The sucrose gradient was separated into 18 fractions calculated by automatic gradient separation system (Biocomp, Canada). The A260 of samples was detected by NanoDrop (Thermo Fisher, USA) to determine the 40-80S or polysome fraction, and RNA was purified from fractions and subjected to RT-qPCR analysis as described above.

2.11. Statistical analysis

Statistical analysis was performed using GraphPad Prism (version 8.2.1). For all experiments with error bars, standard deviation (SD) was calculated and values represent mean ± SD. Presented data are an average of at least three independent experiments ($n \geq 3$) or representative of independent experiments.

Colocalization analysis was performed using ImageJ (version Fiji-win64) and then calculating Person's R value by plugin "Color2".

3. Results and discussion

We first prepared the bio-mimic hydrogel (Fig. 1A) and characterized its mechanical properties(Fig. 1 B&C). Young's modulus and stress relaxation time of hydrogels were measured with nanoindenter. We found negligible differences between multicellular/monolayer formation hydrogel in terms of Young's modulus, both of which fall into range of 5~7 kPa over the mapping area of hydrogel surface (Figs. S1A and S1B). In contrast, the differences of stress relaxation curves between the two types of hydrogel were striking, while the stress of multicellular formation hydrogel performed a more than 50% loss in less than 25s

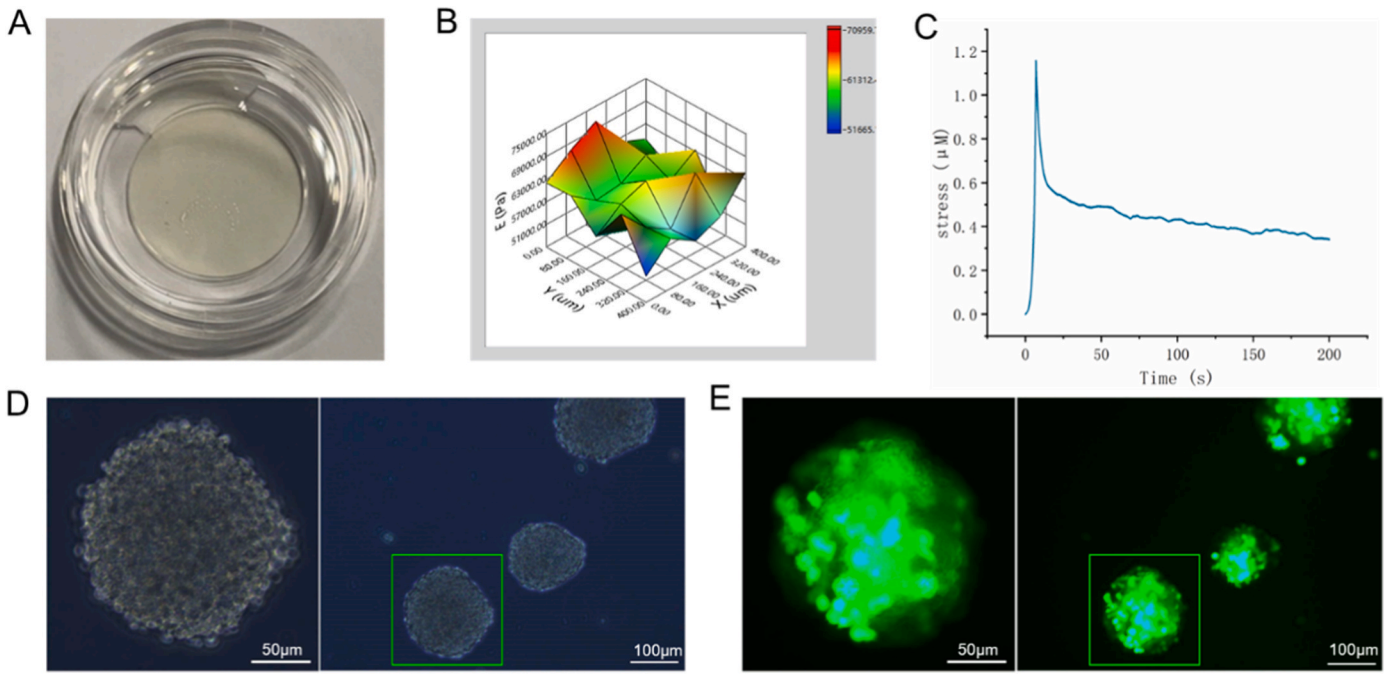

Fig. 1. Characterization of mechanical properties of hydrogel and multicellular formation on the hydrogel. (A–C) Appearance (A), Young's modulus mapping (B), and stress-time curve of hydrogel (C). (D–E) Bright field (D) and fluorescence images (E) of EGFP labeled HEK-293T MCSs formed on the hydrogel after 3 days.

(Fig. S1C), the stress within the monolayer formation hydrogel remained relatively constant over time (Fig. S1D). These data further confirmed our conclusion that by merely controlling the stress relaxation of hydrogel matrices, formation of multicellular spheroids (Fig. S1E) or monolayers (Fig. S1F) can be regulated [12,15]. Indeed, HEK-293T cells formed typical multicellular spheroids (MCSs) when grown on the hydrogel for 3 days (Fig. 1D and E).

To explore the cellular interaction and microenvironment of the MCSs, immunofluorescence staining of the cell-cell adhesion molecule E-cadherin (Fig. 2A), component of the extracellular matrix Fibronectin (FN1, Fig. 2B) and phosphoryl myosin light chain (pMLC) with F-actin (Fig. 2C and D) was carried out. As presented by serial section staining, 3D 293T spheroid cells showed a fully formed cell-cell interactions (Fig. 2A) and elevated endogenous extracellular matrix (Fig. 2B), indicating 293T cells experience a 3D environment provided by the neighboring cells and the ECM. Moreover, 293T MCSs showed enhanced pMLC (Fig. 2C) but a transfer from the adherent surface to the cellular cortex compared to the cells grow on the 2D substrate (Fig. 2D). Since pMLC is indicative of contractility mediated by actomyosin, our results suggest a duration of active mechanic force production and transmission in 293T MCSs [16].

Following the 3D spheroid culture and Shh-N ligand preparation methods described above, spheroid formation by 293T overexpressing Shh-N or control empty vector plasmid were also successfully established, and the Shh-N ligand and control medium were collected respectively (Fig. 3A). The same method was used to obtain Shh-N ligands collected from 2D plate adherent culture and its controls. We used ELISA tests to measure the levels of Shh-N in medium, which were determined in the supernatants collected from 293T cells overexpressing Shh-N cultured in 2D plate adherent and 3D spheroid, respectively. Our results showed that the medium concentration of Shh-N was higher in all experimental groups (both the 2D culture and 3D culture) compared with the respective control groups; at the same time, the level of Shh-N was significantly increased in 3D culture experimental group compared with the 2D culture experimental group (Fig. 3B). And the concentration of Shh-N was not statistically different between the two control groups. 293T cells overexpressing Shh-N treated by 3D culture increase the concentration of Shh-N in the medium, prompting us to further investigate whether Shh-N conditional medium (Shh-N-CM) obtained in this way would change its biologically active phenotype. We further monitored the cell proliferation and found the 293T cells in 3D culture proliferated slowly compared with the cells in 2D plate (Fig. S3A). As shown by Live/Dead assay, after 3 days of 3D culture, 293 MCSs maintained a relative high level of viability (Fig. S3B). The biological activity of Shh-N-CM collected from both cultures (2D plate adherent and 3D spheroid) was testing using WT MEF cells. Treatment methods are as follows: serum-containing medium was removed when MEF cells reached 60–80% confluency, shh-N-CM diluted 1:9 with serum-free culture medium was then added. The results obtained from the RT-qPCR assays showed a significantly higher level of the Gli1 and Ptch1 mRNA in Shh-N-CM treated MEFs collected in 3D culture, similar to the changes in Shh-N levels in the culture medium (Fig. 3B–C). These results demonstrated that Shh signal pathway was activated in Shh-N-CM treated MEFs under 3D environments. There was also a significant increase between the 2D culture group and the 3D culture group when the protein level of Gli1 in Shh-N treated MEFs were examined through western blot (WB) analysis (Fig. 3D).

These results suggest Shh-N ligands obtained in the medium of Shh-N overexpressing 293T cells cultured in spheroid enhanced the response of MEFs to Shh stimulation by increasing the concentration of Shh-N in the conditional medium. To further characterize this enhancement mechanism and also to compare the titers of Shh-N ligands prepared in our laboratory with commercially available Shh-N ligands, we evaluated the ability of various Shh-N ligands to stimulation the activation of the Shh signaling pathway in MEFs, including laboratory prepared and commercial Shh-N ligands. Laboratory prepared and commercially available Shh-N ligands stimulate MEFs according to dilution ratios and concentration gradients, respectively. We examined this activation ability by utilized an artificial Gli reporter system comprised of eight consecutive consensus Gli-binding sites upstream of the luciferase gene. In this system, luciferase expression is then dependent on this promoter, and the expression of luciferase can act as an indicator for measuring the activation of Shh transduction. Luciferase production was dramatically increased in Shh-CM treated MEFs collected from 293T cultured in 3D spheroid compared to Shh-CM treated MEFs collected from 293T cultured in 2D plate adherent. Compared with the Shh-CM collected

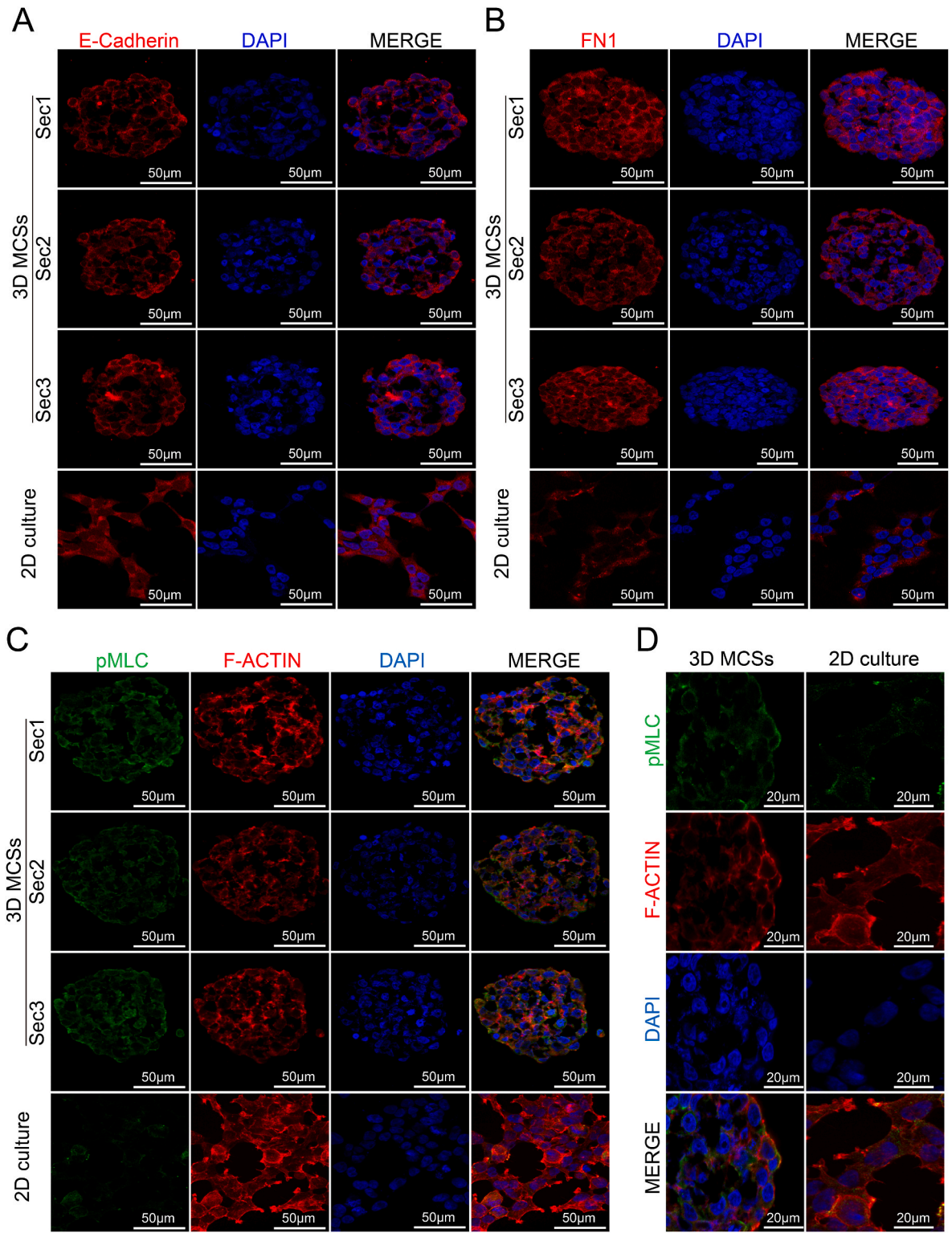

Fig. 2. Serial section fluorescence imaging of 293T multicellular spheroid. Immunostainings of E-Cadherin (red) (A), FN1 (red) (B), phosphor-MLC2 (green) (C and D) and DAPI (blue) on 293T MCSs cryosections. 293T cells cultured on 2D substrate were used as control. Sec1, Sec2 and Sec3 are consecutive sections of the same MCS.

from 293T cultured in 2D plate adherent, the laboratory Shh-N ligand dilution ratio required for maximum activation of the Shh signaling transduction is 1:8, the Shh-CM collected from 3D spheroid culture only needs 1:16, which corresponds to 156.25 ng/ml concentration of commercially available Shh-N ligands (Fig. 3E). Taken together, these data demonstrate that 3D spheroid culture facilitates the production and application of Shh-N ligands.

Shh-N secreted by 293T MCSs upregulates the response of MEFs to Shh prompted us to examine the possible role of Shh-N secreted by 293T MCSs in ciliary regulation. Various regulatory mechanisms of the Shh pathway are known including the *Smo*, which localized to the cilia when cells are stimulated by Shh, and *Gli2* which accumulates at the ciliary tip

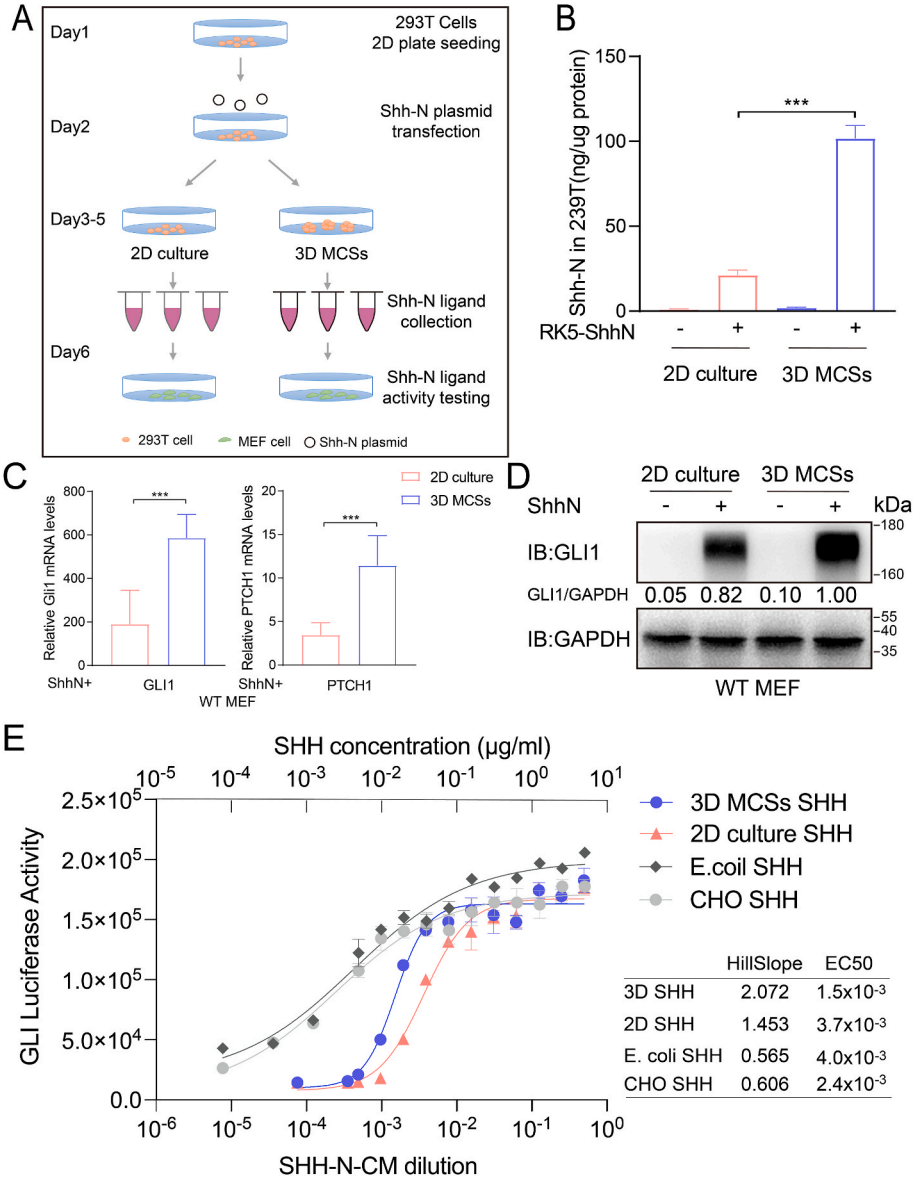

Fig. 3. The secretion of SHH-N and the response of MEFs to SHH were upregulated in 293T MCSs transfected with *Shh-N* plasmid. (A) Flow chart of preparation of SHH-N ligand by using 2D cultured and 3D cultured 293T MCSs. (B) Elisa assays detection of SHH-N secretion in 2D cultured and 3D cultured 293T MCSs. (C) RT-qPCR detection of *Shh* target genes *Gli1* and *Ptch1* mRNA levels in MEF cells. The cells were treated with SHH-N conditional medium collected from 2D cultured and 3D cultured 293T MCSs for 24 h. (D) Western blot analysis of *Gli1* expression in MEF cells treated with SHH-N conditional medium as described in (C). GAPDH was used as an internal control to normalize the protein level of GLI1. (E) Fitted curve representing respective SHH ligand diluted ratio or concentration and corresponding relative luciferase signal intensities. Data in (B, C) were presented as mean ± SD (n ≥ 3). $^{*}P < 0.05$, $^{**}P < 0.01$, $^{***}P < 0.001$.

when stimulated. We assessed if Shh-N secreted by 293T MCSs enhances Shh signaling pathway transduction through *Smo* and *Gli2* entry into the cilia. Specifically, we investigated the endogenous ciliary localizations and localization signal intensity level of *Smo* and *Gli2*, which localized on cilia in response to Shh and representing activation of the Shh pathway. For localization, we found that compared to two controls (2D culture CTRL and 3D MCSs CTRL), cells stimulated by Shh-N whether secreted from 293T 2D plate adherent culture or 3D spheroid culture to form MCSs, the positive rate of ciliary localization of endogenous *Smo* and *Gli2* at the cilia did not change significantly. Confocal microscope indicated that approximately 60% and 50% of Shh-N treated cells had positive signals for *Smo* and *Gli2* localized to cilia, respectively (Fig. 4A–C). Remarkably, different with *Smo*, many cells that had not been treated with Shh-N exhibited positive signal for *Gli2* localization in cilia (Fig. 4A–C). For localization signal intensity level of *Smo* and *Gli2*, in two control cells (2D culture CTRL and 3D MCSs CTRL), there is negligible signal in the cilia. In both Shh-N treated cells (from 2D plate culture and 3D spheroid culture), prominent accumulations of *Smo* and *Gli2* occurs at cilia and cilia tip were observed. Meanwhile, Shh-N secreted from 3D spheroid culture treated cells significantly increased the signal intensity of cilia and ciliary tip localization for *Smo* and *Gli2*, respectively (Fig. 4D–E). Whilst Shh-N secreted by 2D plate adherent culture and 3D spheroid culture treated MEFs did not affect the frequency of *Smo/Gli2*-positive cilia, we did observe a modest increase in *Smo* and *Gli2* positive signal intensity in Shh-N secreted by 293T 3D spheroid culture treated MEFs. Thus, Shh-N secreted by 293T MCSs promotes Shh signaling transduction represented by the accumulation of *Smo* and *Gli2* in cilia and ciliary tips, respectively.

To identify the mechanism why 3D spheroid culture formed MCSs promotes 293T cells overexpressing Shh-N and secreting Shh-N protein, we applied various strategies to explore the role of MCSs in this.

We first briefly examined protein and mRNA changes. We measure the expression of Shh protein that retain only the Sonic Hedgehog N-terminal signaling domain (Shh-N) overexpressing in 293T cells cultured in 2D plate adherent or 3D spheroid culture and observed that there was significant increase in Shh-N protein levels during 3D spheroid culture (Fig. 5A). Moreover, to determine whether this upregulation of Shh-N protein expression is due to increase mRNA levels, we examined the steady-state levels of mRNA for overexpressed Shh-N in both culture conditions (2D plate adherent culture and 3D spheroid culture). The results indicated that this upregulation was not accompanied by changes in steady-state levels of overexpressed Shh-N mRNA (Fig. 5B).

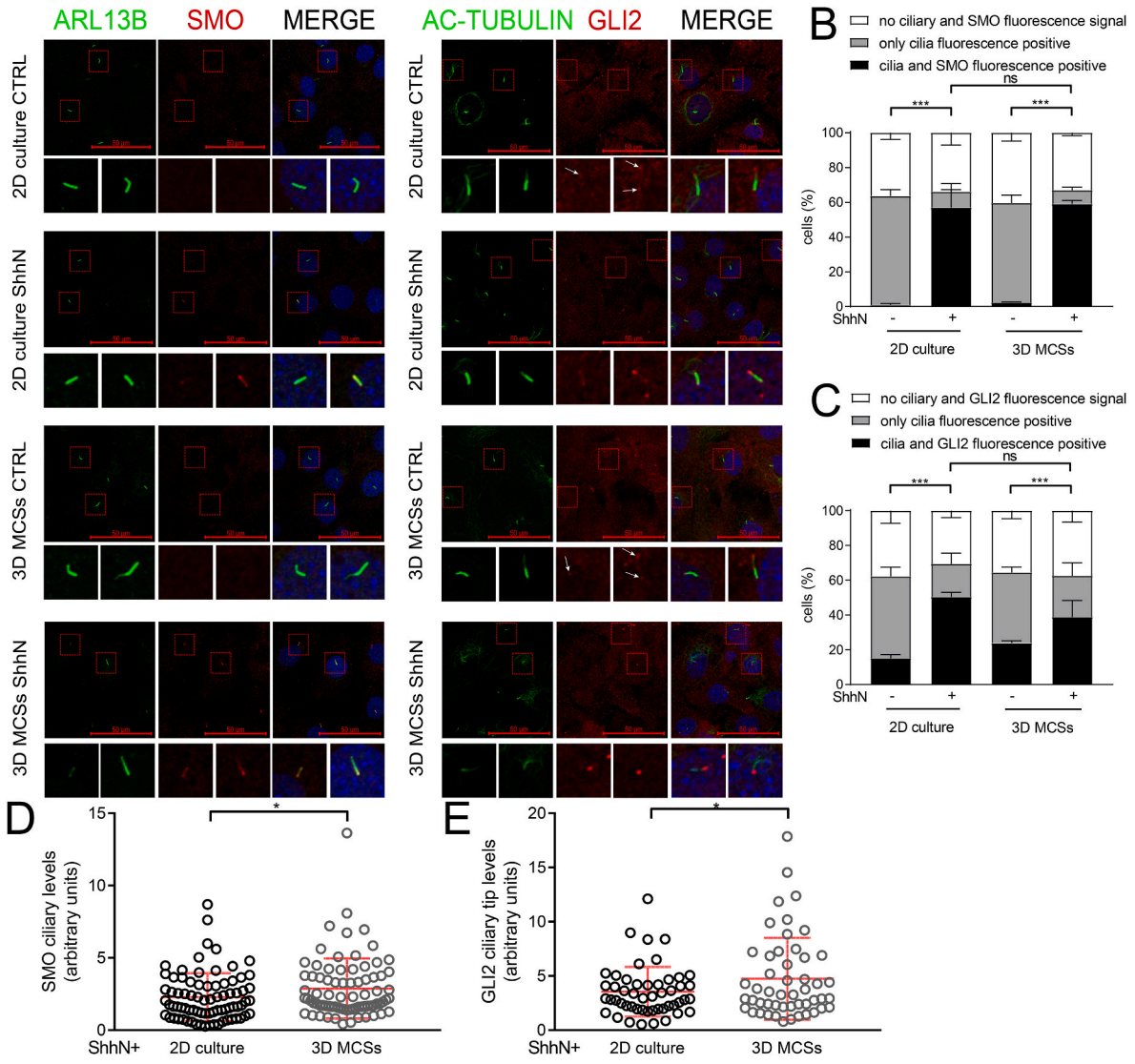

Fig. 4. SHH-N secreted in 293T MCSs promotes *Smo* and *Gli2* accumulation in cilium tips. (A) Representative immunofluorescence images of Shh-induced localization of endogenous *Smo* and *Gli2* at cilium tips in MEF cells. The cells were treated with Shh-N conditional medium collected from 2D cultured and 3D cultured 293T MCSs for 4 h. Quantification showing *Smo*- and *Gli2*-positive cilia (B, C) and the intensity of *Smo* and *Gli2* (D, E) in MEF cells as described in (A). $^{*}P < 0.05$, $^{***}P < 0.001$ (unpaired Student's *t*-test).

Shh is a secreted morphogen and the full length of Shh protein undergoes autocleavage to generate a biologically active N-terminal fragment called Shh-N for secretion. Shh-N interacts with Caveolin-1 (Cav1) to form a protein complex that associates with lipid rafts to complete the secretion process. In vertebrates, extracellular lipid-modified Shh-N protein transduce Shh signaling pathway by binding to downstream receptors. We then focus on the whether this Cav1 promotes lipid transport of Shh-N in MCSs 293T cell was also associated with increased secretion of Shh-N in the medium. Briefly, the expression of Cav1 protein in 293T cells in 2D plate adherent culture and 3D spheroid culture was examined by WB. We observed that 293T cells in 3D MCSs did not increase global cellular Cav1 protein levels (Fig. 5C).

After exploring the possible role of 3D spheroid culture to form MCSs during translation, 293T cells overexpressing Shh-N were culture by 2D plate adherent or 3D spheroid and then subjected by cell whole RNA extraction for polysome profile analysis (Fig. S2A). By using RT-qPCR, the distribution of Shh-N, LaminB1 mRNAs was monitored in polysomes from 2D or 3D cultured 293T cells. (Fig.5D and Fig. S2C). Although we observed that the global cellular translation appears to reduce in 293T MCSs, the relative ratio of 40S subunit/60S subunit/80S ribosome didn't show significant changes between 2D and MCSs cultured 293T cells (Fig. S2B). We consider that this is due to the inconsistency of the total cellular RNA caused by the two culture methods (2D plate adherent culture or 3D spheroid culture). In contrast, polysome distribution of the whole RNA extracted from 293T cells obtained from two culture methods was significantly altered. In the culture through 3D spheroid the distribution of Shh-N mRNA is shifted into heavy ribopolysomes (Fig. 5D). This data demonstrates that Shh-N mRNA enhances the translation process by recruiting ribosomes during 3D spheroid culture to form MCSs, despite 3D spheroid culture reduces the amount of RNA in whole cells. In addition, it has been reported that the activation of eEF1A, which is an essential protein of translation initiation, was regulated by F-actin [17]. Therefore, we performed the immunofluorescence staining (IF) (Fig. 5E) and corresponding statistics (Fig. 5F) demonstrated that the colocalization of eEF1A and F-actin was significantly higher in 3D spheroids than that in 2D. Considering the aforementioned results that expression level was not affected by 3D culture, we concluded the 3D spheroids formation promoted the co-locolization of eEF1A and F-actin.

To investigate the Shh-N protein expression and Shh-CM bioactivity

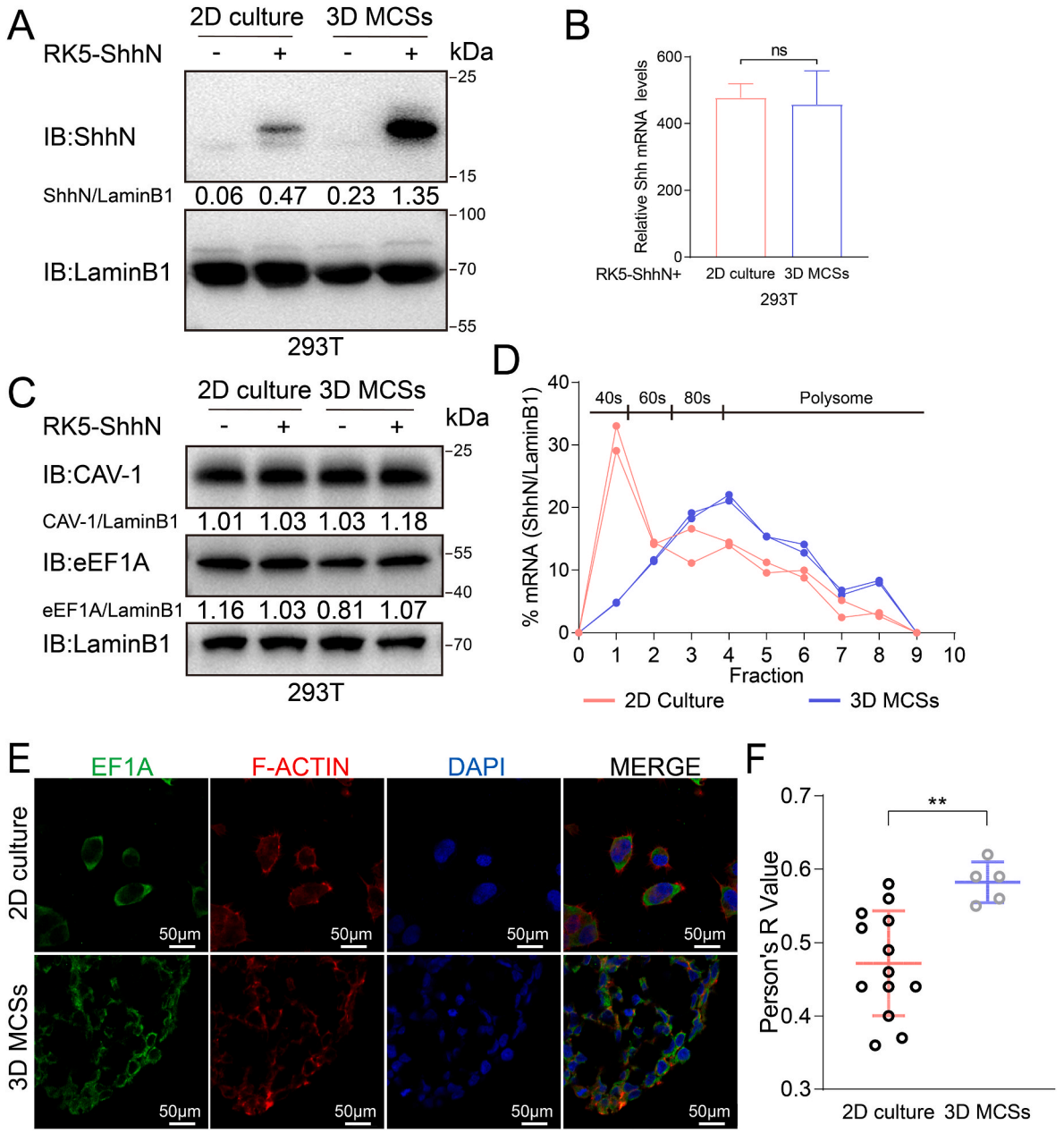

Fig. 5. The formation of MCSs in 293T cells significantly transfers the distribution of overexpressed *Shh-N* mRNA to heavy polyribosomes. (A) Q-PCR detection of *Shh-N* mRNA levels in 2D cultured and 3D cultured 293T MCSs. (B) Western blot analysis of SHH-N expression in 2D cultured and 3D cultured 293T MCSs. LaminB1 was used as an internal control to normalize the protein level of ShhN. (C) Western blot analysis of CAV-1 (Caveolin-1, as a scaffolding protein within caveolar membranes) and eEF1A expression in 2D cultured and 3D cultured 293T MCSs. LaminB1 was used as an internal control to normalize the protein level of CAV-1 and eEF1A. (D) 2D cultured (red) and 3D cultured 293T MCSs (blue) lysates were subjected to polysome profiling, distribution of the *SHH-N* mRNAs relative to that of *LaminB1* is shown as the percent of total mRNA (% mRNA) in each fraction were quantified by RT-qPCR. (E) Immunostainings of eEF1A (green), F-ACTIN (red), phosphor-MLC2 and DAPI (blue) on 2D cultured 293T coverslip and 3D cultured 293T MCSs cryosections. (F) Pearson's R value from colocalization analysis of eEF1A with F-ACTIN (n(2D cultured) = 13, n(3D cultured) = 5, P = 0.0044). Data in (A, C, F) were presented as mean ± SD (n ≥ 3). $^{ns}P \geq 0.05$, $^{*}P < 0.05$, $^{**}P < 0.01$, $^{***}P < 0.001$.

of 293T cells overexpressing Shh-N promoted by active biomaterials with different stiffness, we used two identical active biomaterials with higher stiffness compared to the active biomaterials capable of 3D spheroid culture to form MCSs named B3 and B4 in this article. Both materials behave as elastomers that with negligible stress relaxation under the current test conditions, while the mean Young's modulus of B3 is about twice that of B4 (Figs. S4A and B). Unlike soft active biomaterial, B3 and B4 failed to enable 293T cells to form the observable MCSs (Fig. Szh4C and D). Meanwhile, Shh-N overexpressed protein levels of 293T cells overexpressing Shh-N cultured on B3 and B4 were between those of 293T cells culture in 2D plate adherent and 3D spheroid (Fig. S5A). The stimulatory effect of the generated Shh-CM on MEFs is also the same result (Figs. S5B and C).

As an exocrine protein, the increased secretion of Shh in 293T cells was dependent on the overexpression of Shh promoted by 3D spheroid culture. This result prompted us to further demonstrate this phenotype in other proteins that cannot be excreted, such as PD1 and PDL1 localized in the cell membrane. At the same time, the investigation of the protein expression of PD1 and PDL1 is also with a great meaning at the present time. In immunotherapy, targeting PD1/PDL1 axis can

effectively block its tumor promoting activity. Also, research related to anti-PD1/PDL1 therapy has achieved great advances in the past decade. Anti-PD1 and PDL1 blocks the interaction of PD1 and PDL1, and abolishes the inhibition of $CD8^+$ T cells mediated by this interaction to avert the excessive activation of T cells, thus enhancing the antitumor activity. We followed the experimental strategy above to confirm whether the same mechanism could also be applied to PD1 and PDL1. Specifically, we examined PD1 or PDL1 overexpressed mRNA and protein levels in 293T cells overexpressing PD1 or PDL1 cultured through 2D plate adherent and 3D spheroid respectively and found that the results of both RT-qPCR and WB assays showed that the expression levels of overexpressed PD1 and PDL1 were similar to the changes in expression levels of overexpressed Shh-N in 293T cultured through 3D spheroid (Fig. 6A–D). Remarkably, different with PDL1, endogenous PD1 mRNA levels were significantly reduced in 293T cultured to form MCSs. Our results fail to show changes in protein levels of endogenous PD1 and PDL1 in 293T cells treated with both ways (2D plate adherent culture and 3D spheroid culture). Altogether, our study demonstrates that 293T spheroids provide a novel eukaryotic platform to generate PD1 or PDL1 antigens and might be further utilized to provide new strategies for the production of other proteins. For the future perspective, having the entire platform included in the microfluidic, or organ-on-a-chip model would further improve the yield of proteins. We expect the dynamic culturing environment and shear stress exerted on the cells will provide cells with a mechanobiological environment more similar to *in vivo*, and therefore change the phenotype of cells including protein expression [18].

4. Conclusions

In the present study, we demonstrated the feasibility of a novel mammalian protein expression technique based on a 3D cell culture platform. By adjusting the stress relaxation of 3D matrix hydrogel, 293T significantly increase the expression of various proteins, such as SHH-N, PD-1 or PDL-1 following the formation of spheroids (Fig. 6E). This could

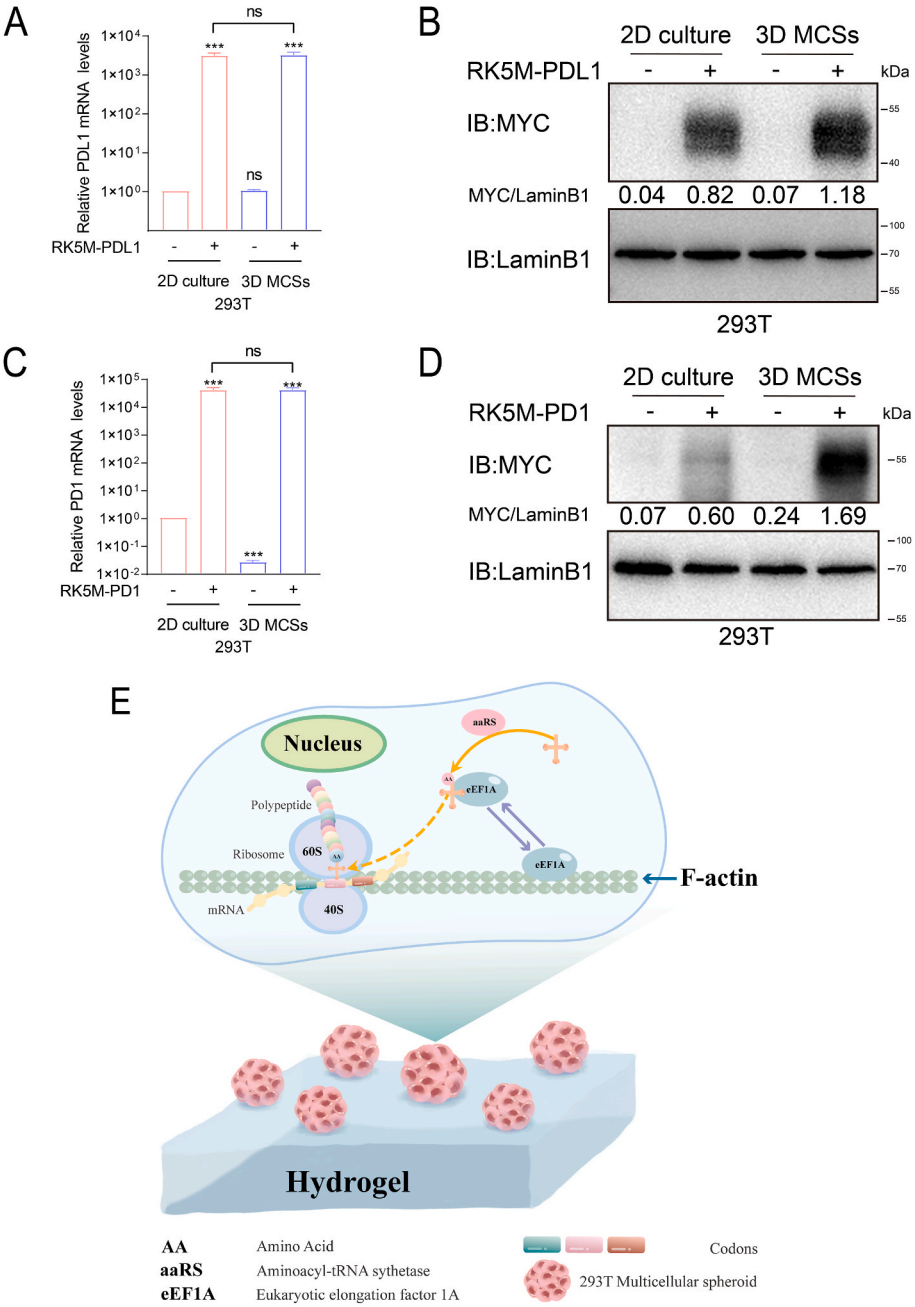

Fig. 6. Increased expression of PDL1 and PD1 in 293T MCSs transfected with *PDL1* and *PD1* plasmid. Q-PCR detection of (A) *PDL1* and (C) *PD1* mRNA levels in 2D cultured and 3D cultured 293T MCSs. Western blot analysis of expression of (B) PDL1 and (D) PD1 with myc-tag at the C-terminus in 2D cultured and 3D cultured 293T MCSs. LaminB1 was used as an internal control to normalize the protein level of PD1 and PDL1. (E) Diagram representation of mechano-biomimetic hydrogel functions to promote efficient mammalian cell protein expression. Data in (A, C) were presented as mean ± SD (n ≥ 3). $^{ns}P \geq 0.05$, $^{*}P < 0.05$, $^{**}P < 0.01$, $^{***}P < 0.001$.

attribute to the increased translation efficiency of yielded protein regulated by cytoskeleton, which were significantly affected during spheroid formation and enhanced the translation process of protein by recruiting ribosomes, eventually results in enhanced protein expression. There is a growing realization that the cytoskeleton not only provides structural support, but also determines the mechanical properties of cells and acts a signaling platform that that regulates the activity and subcellular localization of proteins and organelles. The cytoskeleton closely associates with components of the translational machinery such as ribosomes and elongation factors and, as such, is a crucial determinant of localized protein translation. Taken together, this novel technique can increase cells to express certain proteins in a controllable manner, which demonstrated its potential for cell based large-scale mammalian protein production.

Credit author statement

Yi Zhang and Si-Yang Li: Acquisition of data, Analysis and interpretation of data, Drafting or revising the article; Xing-Ling Li and Jun-Wei Lai: Acquisition of data, Analysis and interpretation of data; Shuo-shuo Sun and Yue Lin: Acquisition of data; Zhao-bin Guo, Ziheng Lv, and Hongxu Meng: Drafting or revising the article; Ke Hu: Conception and design; Acquisition of data, Analysis and interpretation of data, Provision of funding; Ming Xu: Conception and design, Analysis and interpretation of data, Drafting or revising the article, Contributed unpublished essential data or reagents; Ting-ting Yu: Conception and design, Analysis and interpretation of data, Drafting or revising the article.

Declaration of competing interest

The authors declare that they have no known competing financial interests or personal relationships that could have appeared to influence the work reported in this paper.

Data availability

Data will be made available on request.

Acknowledgments

This work was supported by the National Key Research and Development Program of China (No. 2021YFA1201301), National Science Foundation for Young Scientists of China (81703201), the Program of Jiangsu Province Engineering Research Center of Health Emergency (ERCHE2022003), Project Foundation of Jiangsu Cancer Hospital (ZM201924) and the Talent Introduction Foundation of Nanjing Medical University (No. 2017RC07).

Appendix A. Supplementary data

Supplementary data to this article can be found online at https://doi.org/10.1016/j.mtbio.2023.100732.

References

[1] W.C. Merrick, G.D. Pavitt, Cold Spring Harbor Perspect. Biol. 10 (12) (2018) a033092.
[2] K. McDonald. Comprehensive Biotechnology, Second Edition, Academic Press, 2011, pp. 441–449.
[3] J. Yin, G. Li, X. Ren, G. Herrler, J. Biotechnol. 127 (3) (2007) 335.
[4] a) A.R. Aricescu, R. Assenberg, R.M. Bill, D. Busso, V. Chang, S. Davis, A. Dubrovsky, L. Gustafsson, K. Hedfalk, U. Heinemann, Acta Crystallogr. Sect. D Biol. Crystallogr. 62 (10) (2006) 1114.b)G. O. Krasnoselska, M. Dumoux, N. Gamage, H. Cheruvara, J. Birch, A. Quigley, R. J. Owens, in Springer, 2021.
[5] a) K.M. Heffner, Q. Wang, D.B. Hizal, O. Can, M.J. Betenbaugh, Adv. Glycobiotechnol. (2018) 37;
b) J. Zhu, Biotechnol. Adv. 30 (5) (2012) 1158.
[6] M.R. Dyson, Advanced Technologies for Protein Complex Production and Characterization, 2016, 217.
[7] A.D. Bandaranayake, S.C. Almo, FEBS Lett. 588 (2) (2014) 253.
[8] a) R.K. Knaust, P. Nordlund, Anal. Biochem. 297 (1) (2001) 79;
b) S.A. Lesley, Protein Expr. Purif. 22 (2) (2001) 159.
[9] A.M. Vieira Gomes, T. Souza Carmo, L. Silva Carvalho, F. Mendonça Bahia, N. S. Parachin, Microorganisms 6 (2) (2018) 38.
[10] D.R. O'Reilly, L.K. Miller, V.A. Luckow, Baculovirus Expression Vectors: a Laboratory Manual, Oxford University Press on Demand, 1994.
[11] L. Li, J. Eyckmans, C.S. Chen, Nat. Mater. 16 (12) (2017) 1164.
[12] M. Zhang, S. Yan, X. Xu, T. Yu, Z. Guo, M. Ma, Y. Zhang, Z. Gu, Y. Feng, C. Du, Biomaterials 270 (2021), 120687.
[13] X. Yang, N. Jin, Y. Wang, Y. Yao, Y. Wang, T. Li, C. Liu, T. Yu, H. Yin, Z. Zhang, Biochim. Biophys. Acta Mol. Cell Res. 1868 (12) (2021), 119124.
[14] E.S. Pringle, C. McCormick, Z. Cheng, Curr. Protoc. Mol. Biol. 125 (1) (2019) e79.
[15] a) Y. Zhang, L. Peng, K. Hu, N. Gu, Adv. Healthc. Mater. (2022), 2202009;
b) Y. Zhang, Z.b. Guo, Y.m. Nie, G.p. Feng, M.j. Deng, Y.m. Hu, H.j. Zhang, Y. y. Zhao, Y.w. Feng, T.t. Yu, Macromol. Biosci. 22 (4) (2022), 2100498;
c) T. Yu, Y. Hu, G. Feng, K. Hu, Adv. Therapeut. 3 (2020).
[16] a) T.D. Cummins, K.Z. Wu, P. Bozatzi, K.S. Dingwell, T.J. Macartney, N.T. Wood, J. Varghese, R. Gourlay, D.G. Campbell, A. Prescott, J. Cell Sci. 131 (1) (2018), jcs202390;
b) C. Fife, J. McCarroll, M. Kavallaris, Br. J. Pharmacol. 171 (24) (2014) 5507;
c) Z. Guo, C.T. Yang, C.C. Chien, L.A. Selth, P.O. Bagnaninchi, B. Thierry, Small Methods 6 (8) (2022), 2200471;
d) C. Lin, E. Yao, K. Zhang, X. Jiang, S. Croll, K. Peer, P. Chuang, Elife 6 (2017), e21130.
[17] M.B. Mendoza, S. Gutierrez, R. Ortiz, D.F. Moreno, M. Dermit, M. Dodel, E. Rebollo, M. Bosch, F.K. Mardakheh, C. Gallego, Sci. Signal. 14 (691) (2021), eabf5594.
[18] a) Z. Guo, C.T. Yang, M.F. Maritz, H. Wu, P. Wilson, M.E. Warkiani, C.C. Chien, I. Kempson, A.R. Aref, B. Thierry, Adv. Mater. Technol. 4 (4) (2019), 1800726;
b) Z. Guo, N. Zhao, T.D. Chung, A. Singh, I. Pandey, L. Wang, X. Gu, A. Ademola, R.M. Linville, U. Pal, Adv. Sci. (2022), 2204395;
c) L.C. Delon, Z. Guo, A. Oszmiana, C.-C. Chien, R. Gibson, C. Prestidge, B. Thierry, Biomaterials 225 (2019), 119521.